

# A Pseudo-Rigid-Body 3R Model for Determining Large Deflection of Cantilever Beams Subject to Tip Loads

Hai-Jun Su

Assistant Professor

Department of Mechanical Engineering  
University of Maryland, Baltimore County  
1000 Hilltop Circle,  
Baltimore, Maryland 21250  
Email: haijun@umbc.edu

October 30, 2008

## Abstract

*In this paper, a pseudo-rigid-body (PRB) 3R model which consists of four rigid links joined by three revolute joints and three torsion springs is proposed for approximating the deflection of a cantilever beam subject to a general tip load. The large deflection beam equations are solved through numerical integration. A comprehensive atlas of the tip deflection for various load modes is obtained. A three-dimensional search routine has been developed to find the optimal set of characteristic radius factors and spring stiffness of the PRB 3R model. Detailed error analysis has been done by comparing with the pre-computed tip deflection atlas. Our results show that the approximation error is much less than that of the conventional PBR 1R model. The benefits of the PRB 3R model include (a) load independence which is critical for analysis/synthesis applications where loads vary significantly, (b) high accuracy for large deflection beams, and (c) explicit kinematic and static constraint equations which are simpler to solve compared with the finite element model. To demonstrate the use of the PRB 3R model, a compliant 4-bar linkage is studied and verified by a numerical example. The result shows a maximum tip deflection error of 1.2% compared with the FEA model.*

## 1 Introduction

Compliant mechanisms [1] with flexible links that undergo large deflection have many potential advantages such as reduced part number, reduced wear, reduced backlash and error. However the nonlinearity of large deflection beams often complicates analysis and design of compliant mechanisms and prevents its wide applications. One major difficulty comes from the fact that the tip load on the flexible beams of a compliant mechanism, determined by the magnitude of force and moment as well as the force direction, can vary significantly as the mechanism moves. The two extreme cases are when the load is force only (or dominant)

and moment only (or dominant).

Parametric approximation for the beam tip deflection is critical for design synthesis process. Several pseudo-rigid-body (PRB) models have been developed to approximate the tip deflection of flexible beams for various loads. Howell and Midha [2] proposed a PRB 1R model that consists of two rigid links joined at a pin joint and a torsion spring along the beam. Here “R” represents a revolute or pin joint. They have found that the position of the pin joint is determined by the so-called “characteristic radius factor”  $\gamma$  which equals 0.735 for moment only load [3] and 0.85 for force only load [2]. And the equivalent spring stiffness  $K_{\Theta}$  for these two extreme cases are about 1.51 and 2.65 respectively. If the load is a combined end force and end moment,  $\gamma$  and  $K_{\Theta}$  will be anywhere between these two extreme cases. However the approximation error will be significantly large when the tip slope angle is beyond a certain bound, e.g.  $77^{\circ}$  for vertical force loads. Therefore this model is not appropriate for the applications where the load on flexible beams vary significantly or where the load is completely unknown. And it is also not suitable for applications where the mechanism undergoes exceptionally large deflection.

To approximate tip deflection of initially straight cantilever beams subject to combined end force and moment, Saxaena and Kramer [4] modified the PRB 1R model by introducing two linear springs to restrain the change of characteristic radius factor  $\gamma$  for different load modes. Lyon et al. [5] decomposed a flexible beam into two segments, each of which is approximated by a PRB 1R model. However the errors introduced by these two models are exceptionally large. On the other extreme, Saggere and Kota [6] proposed a finite element model that evenly decomposes a flexible beam into  $n \geq 3$  segments joined by  $n$  torsion springs of stiffness  $EI/l$ . This model is completely load independent and can accommodate a wide range of loads. However the approximation accuracy is determined by the number of segments. The larger the number of segments  $n$ , the smaller the approximation error. Unfortunately a large  $n$  can significantly

complicate the kinematic and static equations of compliant mechanisms and slow down the solution process.

By compromising the PRB 1R model and the finite element model aforementioned, this paper proposes a new PRB 3R model for initially straight cantilever beams subject to a combined force and moment. The model is composed of three revolute joints, each accompanied by a torsion spring. The geometric parameters and spring stiffness are independent of external loads. Since the analytical inverse and forward kinematics are readily available for 3R serial chains, the kinematic and static equations are relatively simple.

The rest of paper is organized as follows. In Section 2, large deflection equations of elastic beams are solved by numerical integration in order to generate the complete data set for various end loads which will be used to develop PRB models. Section 3 studies the PRB 1R model for an elastic beam undergoing large deflection. In Section 4, a PRB 3R model for large deflection beams is proposed and analytical kinematics and static equations based on this model are derived. Section 5 studies a load independent PRB 3R model that is optimized to minimize the approximation error. Also in this section detailed error analysis for various loads has been done. In Section 6, a numerical example is provided to demonstrate the benefits of the model and the result is compared with a FEA model. And lastly in Section 7, we discuss the limitation of this model when the approximation error may be large for some load conditions.

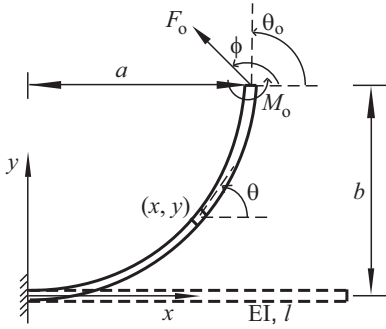


Figure 1: Large deflection of a cantilever beam subject to a combined end force and moment

## 2 Large Deflection Beam Equations

Figure 1 shows an initially straight cantilever beam subject to a combined end force  $F_o$  and moment  $M_o$ . The direction of the end force is denoted by angle  $\phi$ . Parameters  $\theta_o$ ,  $a$  and  $b$  are tip slope angle and the horizontal and vertical tip deflection respectively. The tip deflection of a cantilever beam subject to a general tip load is governed by large deflection

beam theory, calculated as

$$\sqrt{\alpha} = \frac{1}{2} \int_0^{\theta_o} \frac{d\theta}{\sqrt{[\cos(\theta_o - \phi) - \cos(\theta - \phi)] + \kappa}}, \quad (1)$$

$$a/l = \frac{1}{2\sqrt{\alpha}} \int_0^{\theta_o} \frac{\cos \theta d\theta}{\sqrt{[\cos(\theta_o - \phi) - \cos(\theta - \phi)] + \kappa}}, \quad (2)$$

$$b/l = \frac{1}{2\sqrt{\alpha}} \int_0^{\theta_o} \frac{\sin \theta d\theta}{\sqrt{[\cos(\theta_o - \phi) - \cos(\theta - \phi)] + \kappa}}, \quad (3)$$

where  $a/l, b/l$  are normalized tip deflection. And  $\alpha$  and  $\kappa$  are the nondimensional *force index* and *load ratio* respectively defined as

$$\alpha = \frac{F_o l^2}{2EI}, \kappa = \frac{\beta^2}{4\alpha}, \beta = \frac{M_o l}{EI}. \quad (4)$$

The range of the load parameters is discussed as the following. Both the force index and load ratio are non-negative, i.e.  $\alpha \geq 0, \kappa \geq 0$ . Note this incorporates the cases when  $M_o \leq 0$ . The force angle  $\phi$  is between  $[0, 360^\circ]$ . However due to the geometric symmetry, we only need consider the case that the end force  $F_o$  is pointing up, i.e.  $\phi \in [0, 180^\circ]$ . When the end force is downward, the tip deflection in vertical direction will be the same as the upward force cases but with a negative sign.

### 2.1 Numerical Integration of Deflection Equations

Large deflection equations (1-3) consist of three load parameters  $\alpha, \phi, \kappa$  and three tip deflection parameters  $\theta_o, a/l, b/l$ . Given any three parameters, one can find the other three by solving these equations. However it is not convenient to directly solve (1-3) for deflection parameters with known load parameters since the tip slope  $\theta_o$  is one of the integration limits. A common way to overcome this difficult is to solve (1) for  $\alpha$  with a given  $\theta_o$  and then use (2-3) to determine the tip deflection. Howell and Midha [2] provided an elliptic integrals solution and Saxena and Kramer [4] solved these equations with numerical integration. In this article, the numerical integration approach is used to compute tip deflection for various combination of end force and moment.

In this section, we assume that there is not sign change in the curvature of the beam, i.e. the beam slope angle is either monotonically increasing  $\theta \in [0, \theta_o]$  or monotonically decreasing  $\theta \in [\theta_o, 0]$ . Again due to geometric symmetry, we only need considering one case. Without loss of generality, we assume that the beam slope angle is monotonically increasing. In the section 7, we will study the cases when there exists a point of inflection.

When the beam curvature is monotonically increasing, the limit of slope angle  $\theta_{o,max}$  is determined by requiring the term under the square root of equation (1) being positive for  $\theta \in [0, \theta_o]$ , written as

$$\theta_{o,max} = \begin{cases} \phi + \cos^{-1}(1 - \kappa) & : 0 \leq \kappa \leq 2 \\ \infty & : \kappa \geq 2 \end{cases} \quad (5)$$

See [7] for similar results. Choosing values of the parameters  $\theta \in [0, \theta_{o,max}]$ ,  $\phi \in [0, 180^\circ]$  and  $\kappa \in [0, \infty)$ , we can

compute the tip deflection by numerically integrating (1-3). This is done by using the “NIntegrate” function in Mathematica software.

Figure 2 shows the deflected tip loci computed for various load ratios  $\kappa \in [0, 50]$  and various force direction angles  $\phi \in [9^\circ, 171^\circ]$ . Note for simplicity, we set the upper bound of  $\theta_o$  to be  $\pi$ , that is  $\theta_{o,max} = \min[\pi, \phi + \cos^{-1}(1 - \kappa)]$ . All loci start with a circular arc when  $\theta_o$  is small and diverge as the load increases. When the end force dominates the load ( $\kappa < 0.1$ ), the tip locus is straightened out as the load increases. And the smaller the angle  $\phi$ , the earlier this occurs. When the end force and end moment are comparable ( $1 < \kappa < 2$ ), the tip loci diverge significantly for different angles  $\phi$ . The smaller the angle  $\phi$ , the more the loci bend inwards. This is buckling phenomenon caused by axial force dominant loads. As  $\kappa$  increases, the effect of  $\phi$  on the tip locus decreases. When the moment dominates the load ( $\kappa > 5$ ), the tip locus is almost identical to that of pure moment case. Essentially Fig. 2 provides a comprehensive atlas of actual tip deflection which will be used to analyze and compare PRB models.

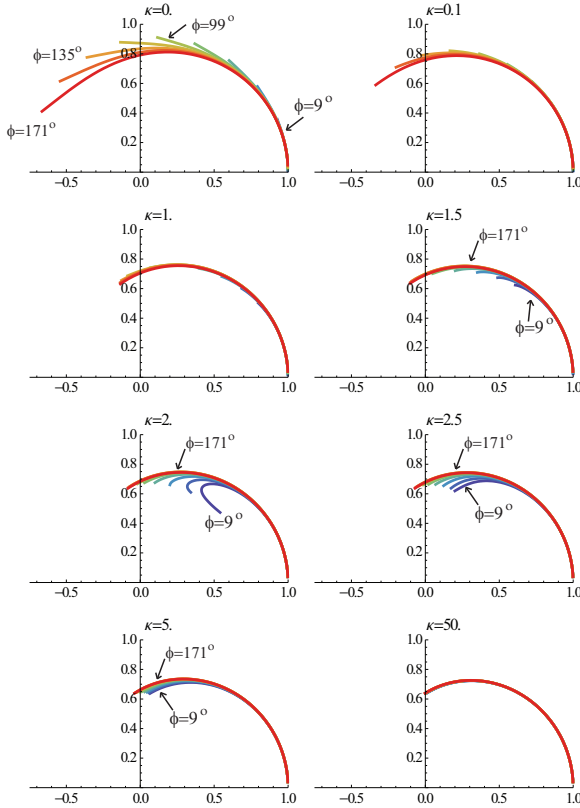


Figure 2: Trajectory of the deflected tip point arranged in terms of load ratio  $\kappa \in [0, 50]$ . The maximum slope angle at the tip is determined by  $\theta_{o,max} = \min[\pi, \phi + \cos^{-1}(1 - \kappa)]$

## 2.2 Limit of Tip Slope Angle by Maximum Stress

Equation (5) gives the upper bound of the end slope angle. In practical designs, the slope angle is often limited by the

maximum stress of the beam which is at the fixed end for a beam with monotonic curvatures [8]. To prevent the beam from failure, the following condition for rectangular section must be satisfied

$$\sigma_{max} \geq \frac{tM_{max}}{2I} = \frac{t}{2I}[M_o + F_o(a \sin \phi - b \cos \phi)], \quad (6)$$

where  $\sigma_{max}$  is the material yield strength and  $t$  is the beam thickness. Substituting the definitions (4) yields

$$\sigma_{max} \geq \frac{Et}{2l}[\beta + 2\alpha\left(\frac{a}{l} \sin \phi - \frac{b}{l} \cos \phi\right)], \quad (7)$$

or

$$2\left(\frac{l}{t}\right)\left(\frac{\sigma_{max}}{E}\right) \geq \beta + 2\alpha\left(\frac{a}{l} \sin \phi - \frac{b}{l} \cos \phi\right) = M_{net}, \quad (8)$$

where the term  $l/t$  (ratio of length to thickness) defines the beam slenderness and  $\sigma_{max}/E$  (ratio of yield strength to Young’s modulus) defines the material flexibility. The larger these two quantities, the larger slope angle the beam can be bent to. The right side of (8)  $M_{net}$  is the normalized net moment applied to the fixed end of the beam.

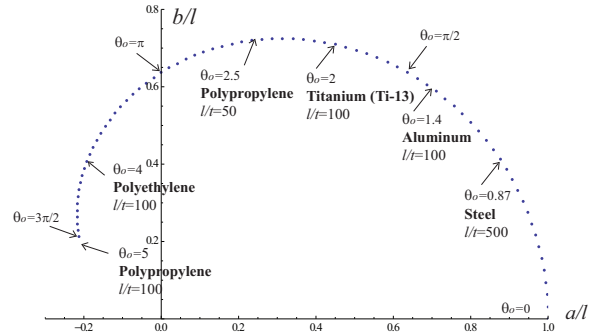


Figure 3: Limit of the tip slope  $\theta_{o,max}$  under pure moment loads determined by maximum stress

Figure 3 shows that  $\theta_{o,max}$  for a flexible beam under moment load is determined by various materials and beam slenderness  $l/t$ . The values of  $\sigma_{max}/E$  for various materials are from page 30 of reference [1]. It can be seen that a polypropylene beam with  $l/t = 100$  can sustain 5 rad or  $286^\circ$  tip bending angle without failure. And steel beams with  $l/t = 500$  can only be bent to an angle of  $50^\circ$ . This figure can help us identify material and slenderness needed for a specific application.

## 3 The Pseudo-Rigid-Body 1R Model

Figure 4 shows the classical PRB 1R model for large deflection beams which is composed of two rigid links connected by a pin joint with a torsion spring. The location of the torsion spring is determined by the characteristic radius factor  $\gamma$ . And the tip point is determined by a PRB angle  $\Theta$ . To

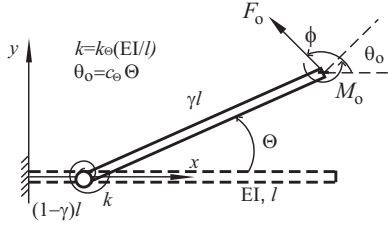


Figure 4: The pseudo-rigid-body 1R model with parameter  $\gamma \in [0.735, 0.85]$  depending on the load

determine  $\gamma$  and  $\Theta$ , Howell and Midha [2] provided a one dimensional search routine that maximizes the angle  $\Theta$  for a prescribed allowable error bound. An alternative way to compute  $\gamma$  and pseudo-rigid-body angle  $\Theta$  for each tip point  $(a/l, b/l)$  is via kinematics of 1R chain, calculated as

$$\gamma = \frac{(1 - a/l)^2 + (b/l)^2}{2(1 - a/l)} \quad (9)$$

$$\Theta = \tan^{-1} \left( \frac{b/l}{a/l + \gamma - 1} \right) \quad (10)$$

It has been shown [4] that  $\gamma$  is predominantly dependent on the load ratio  $\kappa$  and only slightly correlated to force directional angle  $\phi$ . For each load ratio  $\kappa$ , we average the values of  $\gamma$  over  $\phi$  and plot the average value as dots in Fig. 5. We approximate  $\gamma$  versus load ratio  $\kappa$  by the following function

$$\gamma \approx \frac{\gamma_F + 2\gamma_M(c_\gamma\kappa)}{1 + 2c_\gamma\kappa} \quad (11)$$

where  $\gamma_F = 0.842$ ,  $\gamma_M = 0.735$  are the optimal characteristic radius factors for pure end force and for pure end moment respectively. And  $c_\gamma = 4.694$  can be calculated by a standard one parameter linear regression procedure. As far as the author is aware,  $c_\gamma$  has not been previously discussed in the literature. Let us name variable  $c_\gamma$  as “nonlinearity index”.

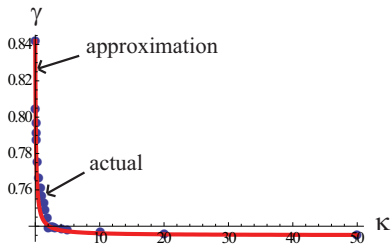


Figure 5: Actual and approximated characteristic radius factor  $\gamma$  vs. load ratio  $\kappa$  for beams under large deflections. The actual values of  $\gamma$  are obtained by averaging over  $\phi \in [0, \pi]$

The approximated values of  $\gamma$  vs.  $\kappa$  is plotted as the continuous line in Fig. 5. The Pearson’s correlation coefficient of the actual value and approximated values is 0.98. They represent errors less than 0.016 or 2%. Comparing with the fitting functions provided in [4] and [9], function (11) is simpler and has a smaller approximation error. Furthermore

function (11) is infinity order continuous for  $\kappa > 0$ , which is important in applying numerical methods for design synthesis [10] and optimization. Similarly the spring stiffness  $k_\Theta$  and the ratio  $c_\Theta$  of the tip slope angle  $\theta_o$  to the PRB angle can be also calculated for each set of  $\theta_o, a/l, b/l$ .

Since the model parameters  $\gamma, k_\Theta, c_\Theta$  are dependent on the load parameters  $\kappa$  and  $\phi$ , it is not convenient for analyzing compliant mechanisms that are subject to a wide range of loads or synthesizing mechanisms when the external load is completely unknown. In what follows, we propose a new 3R model whose geometric parameters and spring coefficients are independent of external loads. We then investigate the accuracy of the model for various load modes.

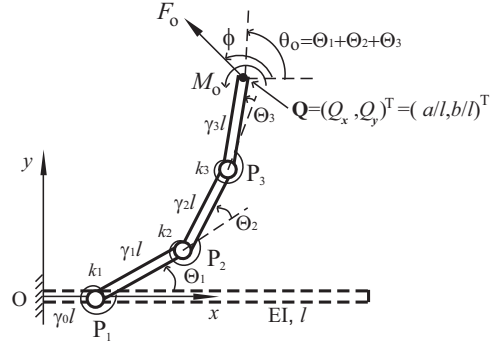


Figure 6: A pseudo-rigid-body 3R model for a cantilever beam subject to a combined end force and moment

## 4 The Pseudo-Rigid-Body 3R Model

Figure 6 shows a PRB 3R serial chain for modeling a flexible beam subject to a combined end force and moment. The PRB model is composed of four rigid links joined by three pin joints and three torsion springs. Let us denote the deflection angles and spring stiffness by  $\Theta_1, \Theta_2, \Theta_3$  and  $k_1, k_2, k_3$  respectively. And the ratio of the four link length to the length of the beam are characteristic radius factors, denoted by  $\gamma_0, \gamma_1, \gamma_2, \gamma_3$  satisfying

$$\gamma_0 + \gamma_1 + \gamma_2 + \gamma_3 = 1. \quad (12)$$

### 4.1 Forward and Inverse Kinematics Equations

The tip point  $\mathbf{Q} = (Q_x, Q_y)^T = (a/l, b/l)^T$  and slope angle  $\theta_o$  of the 3R chain are calculated via its forward kinematics

$$\begin{cases} Q_x = \gamma_0 + \gamma_1 c_1 + \gamma_2 c_{12} + \gamma_3 c_{123} \\ Q_y = \gamma_1 s_1 + \gamma_2 s_{12} + \gamma_3 s_{123} \\ \theta_o = \Theta_1 + \Theta_2 + \Theta_3 \end{cases} \quad (13)$$

where  $c_1 = \cos(\Theta_1), s_1 = \sin(\Theta_1), c_{12} = \cos(\Theta_1 + \Theta_2), s_{12} = \sin(\Theta_1 + \Theta_2), c_{123} = \cos(\Theta_1 + \Theta_2 + \Theta_3), s_{123} = \sin(\Theta_1 + \Theta_2 + \Theta_3)$ .

On the other hand, given tip point  $\mathbf{Q}$  and slope  $\theta_o$ , the PRB angles  $\Theta_i$  are computed by analytical inverse kinematics of the 3R serial chain. The detailed derivation of inverse kinematics of the 3R chain can be found in many textbooks such as Tsai [11]. A sketch of the solution process is shown below. For convenience, we denote the vector from  $\mathbf{P}_1$  to  $\mathbf{P}_3$  by  $\mathbf{P}_{13} = (p_x, p_y)^T$ .

$$p_x = Q_x - \gamma_3 \cos \theta_o - \gamma_0, \quad (14)$$

$$p_y = Q_y - \gamma_3 \sin \theta_o, \quad (15)$$

$$\Theta_2 = \pm \cos^{-1} \left( \frac{p_x^2 + p_y^2 - \gamma_1^2 - \gamma_2^2}{2\gamma_1\gamma_2} \right), \quad (16)$$

$$\Theta_1 = \text{Atan2}(\sin \Theta_1, \cos \Theta_1), \quad (17)$$

$$\Theta_3 = \theta_o - \Theta_1 - \Theta_2, \quad (18)$$

where

$$\cos \Theta_1 = \frac{p_x(\gamma_1 + \gamma_2 \cos \Theta_2) + p_y\gamma_2 \sin \Theta_2}{\gamma_1^2 + \gamma_2^2 + 2\gamma_1\gamma_2 \cos \Theta_2},$$

$$\sin \Theta_1 = \frac{p_y(\gamma_1 + \gamma_2 \cos \Theta_2) - p_x\gamma_2 \sin \Theta_2}{\gamma_1^2 + \gamma_2^2 + 2\gamma_1\gamma_2 \cos \Theta_2}.$$

Note equation (16) yields two solutions, '+' for elbow-down solution and '-' for elbow-up solution. For beams with monotonic curvature, we choose either the elbow-down solution or the elbow-up solution for all  $\theta_o$ .

## 4.2 Statics Equations

Given an external load  $F_o, \phi, M_o$  on the tip of the 3R chain, the torques at the three pin joints are given by

$$\begin{Bmatrix} \tau_1 \\ \tau_2 \\ \tau_3 \end{Bmatrix} = [J^T] \begin{Bmatrix} F_x l \\ F_y l \\ M_o \end{Bmatrix} \quad (19)$$

where we have redefined  $F_x = F_o \cos \phi$ ,  $F_y = F_o \sin \phi$ . And matrix  $[J^T]$  is transpose of the non-dimensional Jacobian of the 3R chain obtained by differentiating kinematic equation (13), written as

$$[J^T] = \begin{bmatrix} -\gamma_1 s_1 - \gamma_2 s_{12} - \gamma_3 s_{123} & \gamma_1 c_1 + \gamma_2 c_{12} + \gamma_3 c_{123} & 1 \\ -\gamma_2 s_{12} - \gamma_3 s_{123} & \gamma_2 c_{12} + \gamma_3 c_{123} & 1 \\ -\gamma_3 s_{123} & \gamma_3 c_{123} & 1 \end{bmatrix}. \quad (20)$$

Let us assume the spring torques are proportional to the PRB angles, i.e.

$$\tau_i = k_i \Theta_i, \quad i = 1, 2, 3, \quad (21)$$

where the spring stiffness  $k_i$  can be normalized into

$$k_i = k_{\Theta_i} (EI/l), \quad i = 1, 2, 3 \quad (22)$$

By substituting definitions (21,22) into (19), we obtain the normalized and nondimensional statics equations:

$$\begin{Bmatrix} k_{\Theta_1} \Theta_1 \\ k_{\Theta_2} \Theta_2 \\ k_{\Theta_3} \Theta_3 \end{Bmatrix} = [J^T] \begin{Bmatrix} 2\alpha \cos \phi \\ 2\alpha \sin \phi \\ \beta \end{Bmatrix}, \quad (23)$$

where the definitions (4) are used.

## 4.3 Computation of Equivalent Spring Stiffness

For a given set of characteristic radius factors  $\gamma_0, \gamma_1, \gamma_2, \gamma_3$ , the spring stiffness  $k_1, k_2, k_3$  are determined in two steps:

1. substitute pre-computed tip point  $a/l, b/l$  and slope  $\theta_o$  (plotted in Fig. 2) into the inverse kinematics equations (14-18) to compute the PRB angles  $\Theta_1, \Theta_2, \Theta_3$  and
2. substitute the angles  $\Theta_1, \Theta_2, \Theta_3$  and load parameters  $\alpha, \beta, \phi$  into (23) to compute the stiffness coefficients  $k_{\Theta_1}, k_{\Theta_2}, k_{\Theta_3}$ .

## 4.4 Three-Dimensional Search for Optimal Characteristic Radius Factors

The PRB 3R model consists of four kinematic parameters  $\gamma_0, \gamma_1, \gamma_2, \gamma_3$  and three static parameters  $k_1, k_2, k_3$ . The goal is to find the optimal model that fits all load modes within an acceptable error range. To achieve this goal, we evenly divide the range of  $\gamma_i \in [0.05, 0.5] (i = 0, \dots, 3)$  with step size 0.05. For any set of  $\gamma_i$ , the spring stiffness are computed for two extreme loads, pure moment and pure vertical force. The optimal set of  $\gamma_i$  is the one which has the minimum difference between the spring stiffness for end moment load and end force load. Because these two load modes represent the extreme cases, the difference of spring stiffness for all other load modes will be guaranteed smaller. Note this is a three dimensional search procedure since the sum of  $\gamma_i$  equals one. The details of the procedure is listed below

1. Pick a set of  $\gamma_i \in [0.05, 0.5] (i = 0, \dots, 3)$ .
2. Compute the equivalent spring stiffness for the end moment load ( $\kappa = \infty, \alpha = 0$ ) using the procedure in Section 4.3 and name them as  $k_{mj} (j = 1, 2, 3)$
3. Compute the equivalent spring stiffness for the vertical end force load ( $\kappa = 0, \phi = \pi/2$ ) and name spring stiffness as  $k_{fj} (j = 1, 2, 3)$
4. Repeat step 2 and 3 for each set of  $\gamma_i \in [0.05, 0.5]$
5. The optimal set of characteristic radius factors is the one in which  $k_{mj}$  is closest to  $k_{fj}$ , that is

$$\left\{ \gamma_i \mid \min \left( \sum_{j=1}^3 (k_{mj} - k_{fj})^2 \right), \gamma_i \in [0.05, 0.5] \right\}$$

To determine the maximum slope angle  $\theta_{o_{max}}$ , we substitute the beam slenderness  $l/t = 100$  and material flexibility  $\sigma_{max}/E = 30$  into equation (8). The search routine found the optimal characteristic radius factors

$$\gamma_0 = 0.1, \gamma_1 = 0.35, \gamma_2 = 0.40, \gamma_3 = 0.15. \quad (24)$$

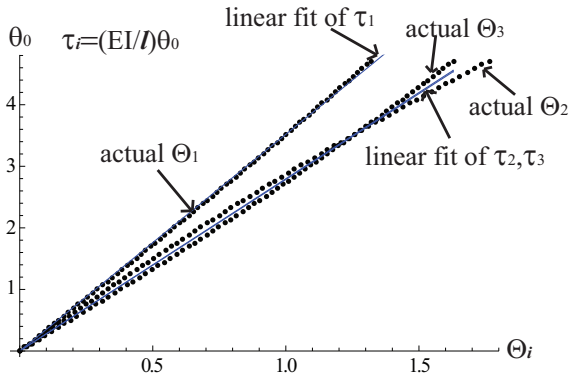


Figure 7: Linear regression of spring stiffness  $k_{\Theta_1}, k_{\Theta_2}, k_{\Theta_3}$  for end moment loads. The range of tip slope angle is  $\theta_o \in [0, 3\pi/2]$

#### 4.5 Evaluation of the PRB 3R Model with a Pure Moment Load

For pure moment loads ( $\kappa = \infty$ ), the actual values of the PRB angles  $\Theta_i$  are plotted as dots in Fig. 7 in which the range of tip slope is  $\theta_o \in [0, 3\pi/2]$ . A linear regression process is used to compute the approximated values of spring stiffness  $k_{\Theta_1}, k_{\Theta_2}, k_{\Theta_3}$  as

$$k_{\Theta_1} = 3.51933, k_{\Theta_2} = 2.78518, k_{\Theta_3} = 2.79756. \quad (25)$$

The linear fit curves are plotted as continuous lines in Fig. 7.

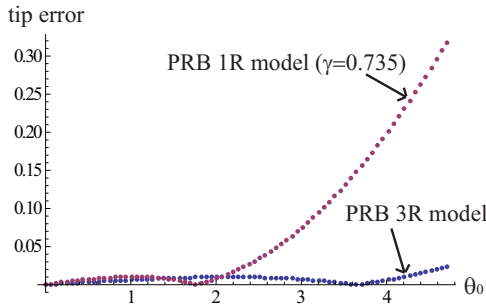


Figure 8: Comparison of the tip error of PRB 1R model with the PRB 3R model for beams under moment loads

The error of tip locus of the PRB 3R model is plotted in Fig. 8. The maximum error of the tip deflection is 2.3% of beam length for  $\theta_o \in [0, 3\pi/2]$ . And the relative error of the tip slope angle is given by

$$|1/k_{\Theta_1} + 1/k_{\Theta_2} + 1/k_{\Theta_3} - 1| = 0.064\% \quad (26)$$

As a comparison, the PRB 1R model gives an error of 31.8% for tip locus and an error of 25.8% for tip slope angle at  $\theta_o = 3\pi/2$ . When using PRB 1R model, the slope angle must be limited below  $100^\circ$ . Figure 9 shows the tip loci of the PRB 1R model and PRB 3R model. It can be seen that the PRB 1R model deviates off the actual curve when

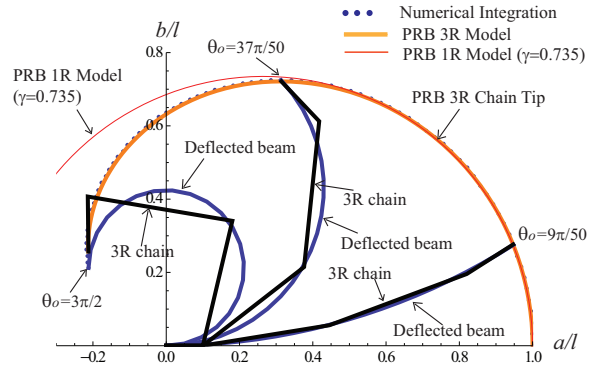


Figure 9: Comparison of the tip loci of the PRB 1R model and the PRB 3R Model for beams under moment loads.

$\theta_o > 120^\circ$ , while the PRB 3R model is still accurate. The shape of the deflected beam and corresponding configuration of the PRB 3R chain at three representative positions  $\theta_o = 9\pi/50, \theta_o = 37\pi/50, \theta_o = 3\pi/2$  are also plotted in Fig. 9.

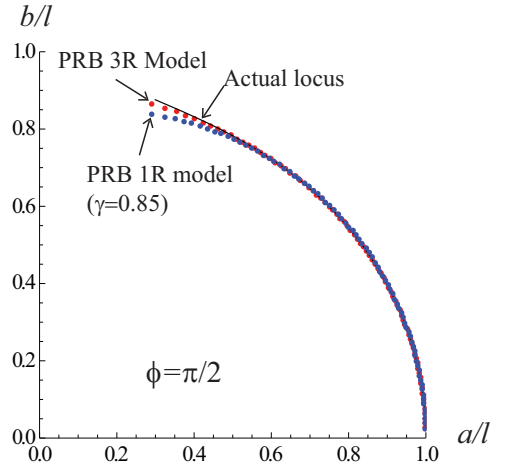


Figure 10: Comparison of tip locus of the PRB 1R model and the PRB 3R Model for beams under force loads.

#### 4.6 Evaluation of the PRB 3R Model with a Pure Force Load

Similarly the spring stiffness are computed for the pure force load ( $\kappa = 0$ ) as

$$k_{\Theta_1} = 3.71591, k_{\Theta_2} = 2.87128, k_{\Theta_3} = 2.26417, \quad (27)$$

where the characteristic radius factors in (24) are used and the maximum tip slope angle is  $\theta_o = \phi$  by Eq. (5). Figure 10 shows the tip loci of PRB 1R model and the PRB 3R model for beams under a vertical force load ( $\phi = \pi/2$ ). Once again, the PRB 3R model has a smaller error of 1.2% than the error of 3.6% for PRB 1R model at  $\theta_o = \pi/2$ .

Table 1: Geometric parameters and equivalent spring stiffness of the optimized PRB 3R model

$\gamma_0 = 0.1, \gamma_1 = 0.35, \gamma_2 = 0.40, \gamma_3 = 0.15$
$k_1 = 3.51 \frac{EI}{l}, k_2 = 2.99 \frac{EI}{l}, k_3 = 2.58 \frac{EI}{l}$

## 5 The Optimal PRB 3R Model

The goal of this section is to find the optimal PRB 3R model that best fits the theoretical tip deflection atlas for a wide range of external loads. For the optimal set of  $\gamma_i$  given in (24), we plot the spring stiffness  $k_{\Theta_1}, k_{\Theta_2}, k_{\Theta_3}$  vs.  $\phi \in [0, \pi]$  with  $\kappa = 0$  in Fig. 11(a). It can be seen that the spring stiffness is only slightly correlated to force direction angle  $\phi$ . Hence the effect of  $\phi$  can be neglected in finding the desired load independent model.

Figure 11(b) shows the plot of the spring stiffness vs.  $\kappa \in [0, 25]$  with fixing  $\phi = \pi/2$ . The spring stiffness  $k_{\Theta_1}$  drops from 3.716 at  $\kappa = 0$  to 3.445 at  $\kappa = 5$  and then remains constant. Similarly  $k_{\Theta_2}$  increases from 2.871 at  $\kappa = 0$  to 3.031 at  $\kappa = 5$  and then remains constant. However  $k_{\Theta_3}$  suffers a sharp increase from 2.264 at  $\kappa = 0$  to 2.600 at  $\kappa = 0.1$  and then flattens out.

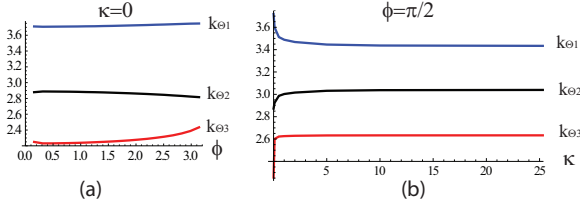


Figure 11: (a) Plot of stiffness  $k_{\Theta_i}$  vs. the force directional angle  $\phi \in [0, \pi]$  for  $\kappa = 0$  and (b) Plot of stiffness  $k_{\Theta_i}$  vs. the load ratio  $\kappa \in [0, 25]$  for  $\phi = \pi/2$

The spring stiffness for the final optimal PRB 3R model is computed by averaging over  $\kappa \in [0, 25]$ . The kinematic and static parameters of the optimal PRB 3R model are summarized in Table 1.

### 5.1 Comparison of the Optimal PRB 3R Model with the Results of Numerical Integration

The error analysis of the optimal PRB 3R model is carried out via the following three steps:

1. compute the PRB angles  $\Theta_1, \Theta_2, \Theta_3$  for a given external load  $\alpha, \phi, \beta$  by solving the static equations (23),
2. compute the tip point  $a/l, b/l$  and tip slope angle  $\theta_o$  with PRB angles computed from step 1 by forward kinematics (13) and
3. compute error of the tip point and slope angle with the numerical integration solution plotted in Fig. 2.

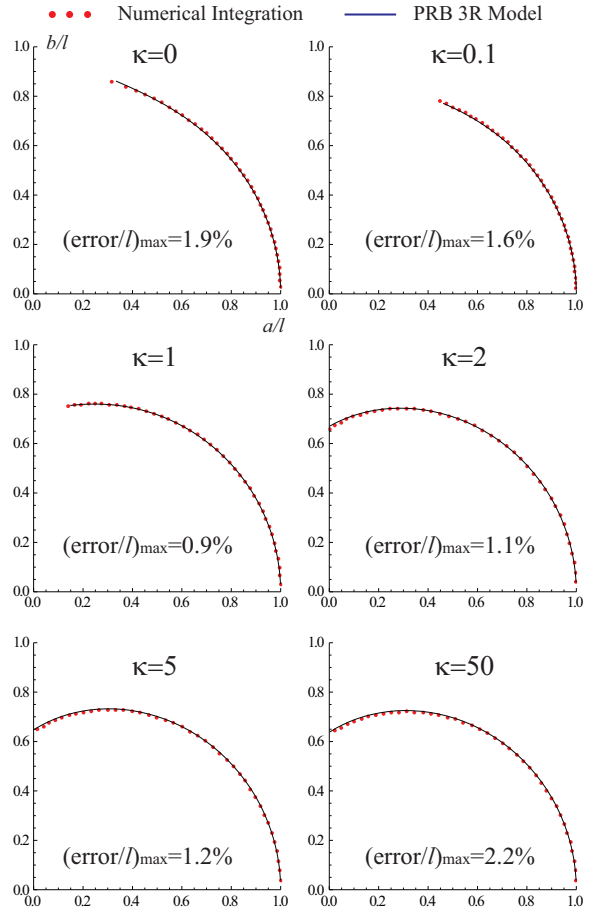


Figure 12: Approximation error of the PRB 3R model for various load indices  $\kappa$  with  $\phi = \pi/2$ . Dots represent the deflection loci computed via numerical integration and the solid lines represent the approximated tip loci predicted the optimal PRB 3R model.

Figure 12 shows the actual and approximated tip loci for different load indices  $\kappa$  with fixed force angle  $\phi = \pi/2$ . The maximum error for the tip point is about 2.2% of the beam length. And Fig. 13 shows the actual and approximated tip loci for different force angles  $\phi$  with fixed load ratio  $\kappa = 0$ . The maximum error of tip is about 8.5% when  $\phi = 175^\circ$  which corresponds to the maximum tip slope angle  $\theta_{o,max} = 153^\circ$ .

The most difficult load mode to approximate is when  $\kappa = 2$  and  $\phi$  is small (Fig. 2). This corresponds to a load in which the moment is comparable with an axially dominant force. For this case, tip deflection angles must be constrained below a certain value in order to maintain a certain error bound.

### 5.2 Analysis of a Compliant Four-Bar with the PRB 3R Model

To demonstrate the use of the proposed PRB 3R model in analyzing compliant mechanisms, here we study a compliant four-bar linkage shown in Fig. 14. The crank link OA is hinged to the ground at the pint joint B and to the coupler

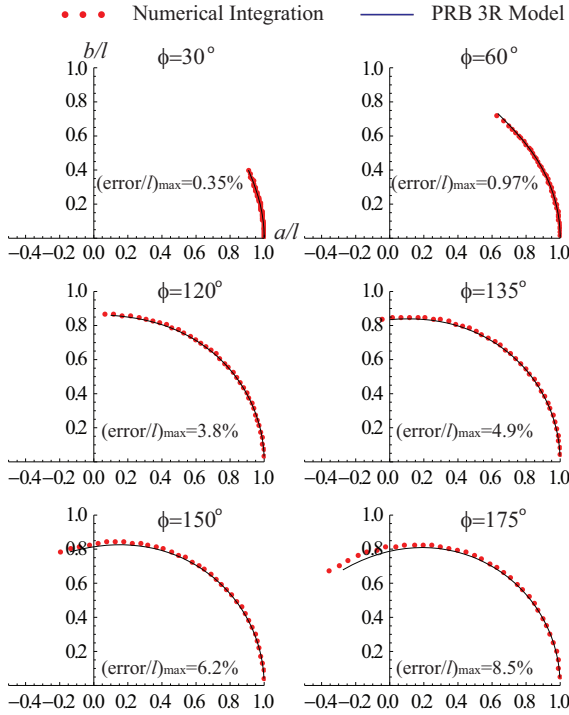


Figure 13: Approximation error of the PRB 3R model for various force direction angles  $\phi$  with fixed load ratio  $\kappa = 0$ . Dots represent the actual deflection loci computed via numerical integration and the solid lines represent the approximated tip loci predicted by the optimal PRB 3R model.

link AQ at the pin joint **A** respectively. Links OA and AQ are considered rigid. The follower link OQ is initially straight and considered flexible with one end fixed on the ground and the other end rigidly connected to the coupler link AQ at the point **Q**.

The coordinate systems are defined as the following. The origin of the global coordinate system  $xy$  is chosen at the fixed end of the flexible beam with the  $x$  axis along the beam. For convenience, a moving coordinate system  $uv$  is placed on the coupler link at the connection point **Q** with the  $u$  axis along the slope of the beam tip. Let  $\mathbf{Q} = (Q_x, Q_y)^T$ ,  $\mathbf{B} = (B_x, B_y)^T$  and  $\mathbf{A} = (A_x, A_y)^T$  denote the coordinates of the points **Q**, **B**, **A** respectively. The length and position of the crank link are denoted by  $r$  and the angle  $\psi$  respectively. The position of the pin joint **A** in the moving frame system are denoted  $(A_u, A_v)^T$ .

The kinematic constraint equations are obtained by applying the loop closure at the pin joint **A**, written as

$$\begin{Bmatrix} Q_x \\ Q_y \end{Bmatrix} + \begin{bmatrix} c_{123} & -s_{123} \\ s_{123} & c_{123} \end{bmatrix} \begin{Bmatrix} A_u \\ A_v \end{Bmatrix} = \begin{Bmatrix} B_x \\ B_y \end{Bmatrix} + r \begin{Bmatrix} \cos \psi \\ \sin \psi \end{Bmatrix}, \quad (28)$$

And the coordinates of the beam tip **Q** can be written in terms of three pseudo rigid angles via the forward kinematics (13).

We disconnect the follower link and the coupler link at the point **Q** and define the internal force and moment applied

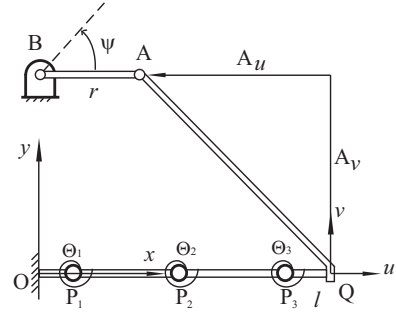


Figure 14: A compliant four-bar linkage formed by a fixed-flexible beam OQ and two rigid links BA and AQ connected by two pin joints **A** and **B**.

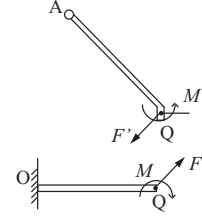


Figure 15: The internal force and moment at the connection point **Q**.

to the beam OQ at the point **Q** as  $\mathbf{F} = (F_x, F_y)^T$  and  $M$  respectively. See Fig. 15. They can be obtained by solving equation (19)

$$\begin{Bmatrix} F_x l \\ F_y l \\ M \end{Bmatrix} = [J^T]^{-1} \begin{Bmatrix} k_1 \Theta_1 \\ k_2 \Theta_2 \\ k_3 \Theta_3 \end{Bmatrix}, \quad (29)$$

where inverse of the matrix (20) can be derived analytically and written as

$$[J^T]^{-1} = \begin{bmatrix} \gamma_2 c_{12} & -\gamma_1 c_1 - \gamma_2 c_{12} & \gamma_1 c_1 \\ \gamma_2 s_{12} & -\gamma_1 s_1 - \gamma_2 s_{12} & \gamma_1 s_1 \\ \gamma_2 \gamma_3 s_3 & -\gamma_3 (\gamma_2 s_3 + \gamma_1 s_{23}) & \gamma_1 (\gamma_2 s_2 + \gamma_3 s_{23}) \end{bmatrix} / (\gamma_1 \gamma_2 s_3) \quad (30)$$

The static equilibrium equation is obtained by vanishing the resultant moment of the reaction force  $\mathbf{F}'$  and  $M'$  with respect to the pin joint **A**, written as

$$\mathbf{A}\mathbf{Q} \times \mathbf{F}' + M' \mathbf{k} = 0, \quad (31)$$

where the symbol “ $\times$ ” represents the vector cross product and  $\mathbf{A}\mathbf{Q} = (AQ_x, AQ_y)^T$  is the vector from the point **A** pointing to the point **Q**, calculated from (28) as

$$\begin{Bmatrix} AQ_x \\ AQ_y \end{Bmatrix} = \begin{Bmatrix} Q_x \\ Q_y \end{Bmatrix} - \begin{Bmatrix} A_x \\ A_y \end{Bmatrix} = - \begin{bmatrix} c_{123} & -s_{123} \\ s_{123} & c_{123} \end{bmatrix} \begin{Bmatrix} A_u \\ A_v \end{Bmatrix} \quad (32)$$

By using the fact that  $\mathbf{F}' = -\mathbf{F}$  and  $M' = -M$ , Eq. (31) can be re-written in scalar form as

$$AQ_x F_y - AQ_y F_x + M = 0. \quad (33)$$

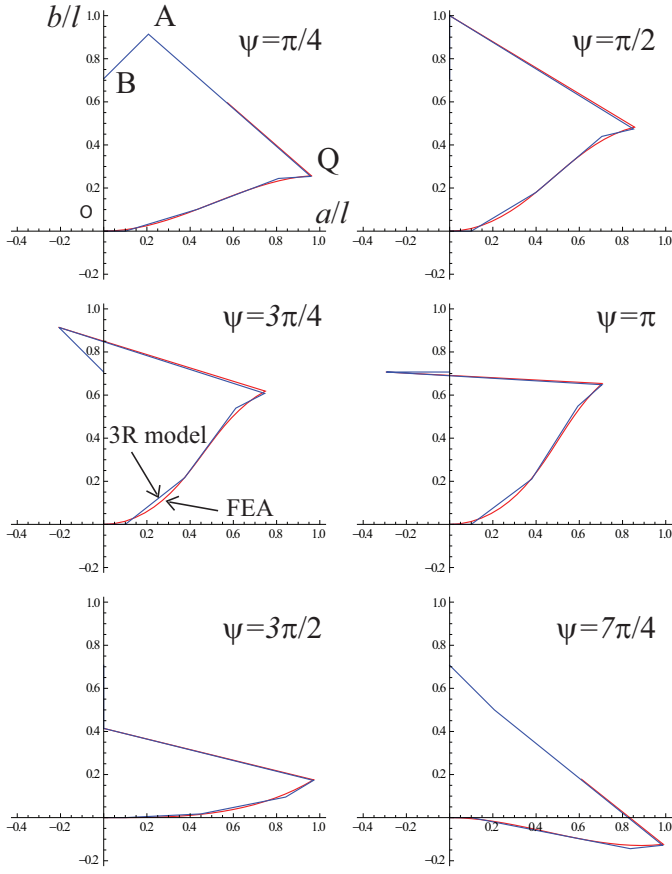


Figure 16: Plots of the deflection of a partially compliant 4-bar mechanism computed by the optimized PRB 3R model and by the FEA model with the input crank  $\psi \in [0, 2\pi]$ .

Substituting (29) and (32) into (33) and combining with the kinematic constraint equations (28) yield a system of three equations in three unknowns  $\Theta_1, \Theta_2, \Theta_3$ . Assuming the crank angle  $\psi$  is controlled, we can then apply numerical solvers such as Newton-Raphson based iteration method to obtain solutions of  $\Theta_1, \Theta_2, \Theta_3$ . It can be seen that the kinematic and static equations are much simpler compared with the finite element model where a large number of nonlinear equations must be solved.

Note it is possible to transfer the resulted equations into a polynomial form by using the approximation techniques proposed by Su and McCarthy [12] and analytically solve the polynomial system to obtain solutions. However this is out of the scope of this paper and shall be an interesting research topic in the future.

## 6 A Numerical Example

Consider the partially compliant 4-bar shown in Fig. 14 and let  $A_u/l = -1/\sqrt{2}$ ,  $A_v/l = 1/\sqrt{2}$ ,  $r/l = 1 - \sqrt{2}/2$ ,  $\mathbf{B} = (0, 1/\sqrt{2})$ . By driving the crank angle  $\psi \in [0, 2\pi]$ , the motion of the flexible beam and the coupler link is determined by simultaneously solving the kinematic constraint equations (28)

and the static constraint equation (33). The linkage at six key positions is plotted as blue lines in Fig. 16. To verify the results, a finite element analysis (FEA) model is built with ABAQUS software. The crank link and coupler link are defined as discrete rigid element and the flexible follower link OQ is meshed into 20 planar beam elements. The linkage based on the FEA model is plotted as red lines Fig. 16.

It can be seen that the deformation of the PRB 3R model is very close to the FEA model. To find the accuracy of the PRB 3R model, we calculate the normalized tip error relative to the FEA model and plot it in Fig 17. It can be seen that a maximum tip error is about 1.2% of the beam length for  $\psi \in [0, 2\pi]$ , which is acceptable for conceptual design stage. Please note that there is no error for force parameters as the tip deflection is calculated with the actual force applied on the beam. In other words, all errors are attributed to the errors of the tip and slope deflection.

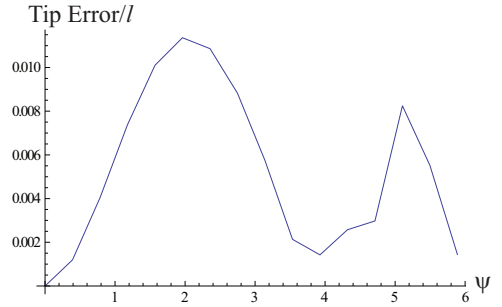


Figure 17: Tip error of the optimized 3R model compared with the FEA model for  $\psi \in [0, 2\pi]$

## 7 Limitations

The parameters  $\gamma_j, k_i$  of the proposed PRB 3R model are only dependent on the geometry and material of the beam and but not on the external load. However several limitations for the proposed PRB 3R model should be pointed out. First of all, when the end force is axially dominant, i.e.  $\phi$  is close to  $0^\circ$  or  $180^\circ$ , the end slope angle  $\theta_o$  must be limited within a certain range in order to have an accurate approximation. In this article, the force angle is limited to  $\phi \in [9^\circ, 171^\circ]$ .

In section 2.1, we assumed that there is no inflection point in the deflected beam. Here we study the accuracy of the PRB 3R model for configurations with a point of inflection. Obviously the end moment must be clockwise, i.e.  $M_o \leq 0$  for this case. At the inflection point, the beam curvature is zero, i.e.  $d\theta/ds = 0$  or

$$\cos(\theta_o - \phi) - \cos(\theta_i - \phi) + \kappa = 0 \quad (34)$$

where  $\theta_i$  is the slope angle at the point of inflection. Alternatively  $\theta_i$  can be expressed as

$$\theta_i = \phi + \cos^{-1}(\cos(\theta_o - \phi) + \kappa) \quad (35)$$

The inflection angle  $\theta_i$  exists only when  $|\cos(\theta_o - \phi) + \kappa| \leq 1$ . Since  $\cos(\theta_o - \phi)$  is bounded, there does not exist an

inflection point for the load with  $\kappa > 2$ . And the inflection slope angle is always greater than the tip slope angle, i.e.  $\theta_i > \theta_o$ .

When a point of inflection exists, the functions of the integration (1-3) are discontinuous at  $\theta = \theta_i$ . Therefore the deflection equations must be modified as

$$\sqrt{\alpha} = \frac{1}{2} \left( \int_0^{\theta_i} \frac{d\theta}{\sqrt{[\cos(\theta_o - \phi) - \cos(\theta - \phi)] + \kappa}} + \int_{\theta_o}^{\theta_i} \frac{d\theta}{\sqrt{[\cos(\theta_o - \phi) - \cos(\theta - \phi)] + \kappa}} \right) \quad (36)$$

$$a/l = \frac{1}{2\sqrt{\alpha}} \left( \int_0^{\theta_i} \frac{\cos \theta d\theta}{\sqrt{[\cos(\theta_o - \phi) - \cos(\theta - \phi)] + \kappa}} + \int_{\theta_o}^{\theta_i} \frac{\cos \theta d\theta}{\sqrt{[\cos(\theta_o - \phi) - \cos(\theta - \phi)] + \kappa}} \right) \quad (37)$$

$$b/l = \frac{1}{2\sqrt{\alpha}} \left( \int_0^{\theta_i} \frac{\sin \theta d\theta}{\sqrt{[\cos(\theta_o - \phi) - \cos(\theta - \phi)] + \kappa}} + \int_{\theta_o}^{\theta_i} \frac{\sin \theta d\theta}{\sqrt{[\cos(\theta_o - \phi) - \cos(\theta - \phi)] + \kappa}} \right) \quad (38)$$

For given values of  $\phi$  and  $\theta_o$ , we choose values of  $\theta_i \in [\theta_o, \theta_o + \delta\theta]$ . The load ratio  $\kappa$  must be chosen such that  $\cos(\theta_o - \phi) - \cos(\theta_i - \phi) + \kappa \geq 0$  for all  $\theta \in [0, \theta_i]$ . For instance we choose the minimum value for  $\kappa$ , i.e.  $\kappa = \cos(\theta_i - \phi) - \cos(\theta_o - \phi)$ . Computing the integrations (36-38) obtains the tip deflection. Figure 18 shows the comparison of the results of the PRB 3R model (black solid line segments) and the numerical integration (blue continuous lines). The deformation of the PRB 3R model is computed by solving the static equations (23) with any given end force  $\alpha, \phi, \beta$ .

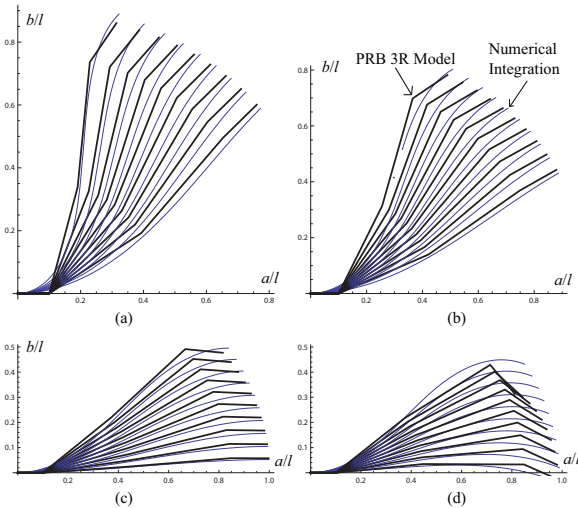


Figure 18: Comparison of large deflection beams with an inflection point (a)  $\theta_o = \pi/4$  (b)  $\theta_o = \pi/6$ , (c)  $\theta_o = 0$ , (d)  $\theta_o = -\pi/8$

Figure 18(a) shows the cases of  $\phi = \pi/2, \theta_o = \pi/4$  and  $\theta_i \in [11\pi/40, 19\pi/40]$ . For these cases, the maximum tip error is 3.02% of the beam length. Figure 18(b) shows the

cases of  $\phi = \pi/2, \theta_o = \pi/6$  and  $\theta_i \in [23\pi/120, 5\pi/12]$  with a maximum tip error of 2.75%. The configurations of the 3R chain are all elbow down, i.e.  $\Theta_2 > 0$ . Figure 18(c) shows the cases of  $\phi = \pi/2, \theta_o = 0$  and  $\theta_i \in [\pi/40, \pi/4]$  with a maximum tip error of 2.92%. The second PBM angle is close to zero, i.e.  $\Theta_2 \approx 0$ . It can be seen that the errors are sufficiently small for the cases with positive and zero tip slope angle  $\theta_o \geq 0$ .

However when the beam tip is bent downwards, i.e.  $\theta_o < 0$ , the configuration of the 3R chain will be elbow up, i.e.  $\Theta_2 < 0$ . This is shown in Fig. 18(d) where  $\phi = \pi/2, \theta_o = -\pi/8$  and  $\theta_i \in [\pi/40, \pi/4]$ . The maximum error is 12.3% of the beam length when  $\theta_i = \pi/4$ . For this kind of load, the inflection angle, hence the end moment must be limited.

## 8 Conclusion

This paper proposes a pseudo-rigid-body 3R model analyzing/synthesizing large deflection of cantilever beams subject to combined end force and moment. The model is a planar serial chain with three revolute joints, each accompanied with a torsion spring. The deflection of flexible beams depends on three load parameters: force index, force direction angle and load ratio. Numerical integration is used to compute the actual beam deflection (tip point and tip slope) for various load modes. These three dimensional data sets are then input to a three dimensional search routine in order to find the optimal kinematic parameters (characteristic radius factors) and static parameters (spring stiffness). The result is a 3R serial chain model with parameters independent of external loads. The error analysis for various load modes shows that this model is accurate and can accommodate a wide range of load ratios, force direction angles and tip slope angles.

Lastly a compliant mechanism example is used to demonstrate how to use the proposed PRB 3R in analyzing compliant mechanisms. A numerical example is provided and compared with the result of a FEA model. The result shows a maximum tip error of 1.2% when the optimized PRB 3R is used. This model is an important contribution to the field and is very suitable for kinematic/static synthesis leading to the conceptual design of compliant mechanisms.

However one should be aware about the limitations of this model. The approximation error of this model will be significantly large for some extreme load conditions such as axially dominant forces and the cases when the beam has an inflection point and the slope angle is bent downwards. Further studies will be needed for these cases. In addition, it is anticipated that extra complexity will be introduced into the synthesis equations when this 3R model is used.

## Acknowledgment

The author wishes to express his thanks to anonymous reviewers for their insightful comments and to Mr. Kun He

and Mr. Fenqi Luo from Department of Mechanical Engineering, University of Maryland, Baltimore County for their help with using ABAQUS software. This research is sponsored by the UMBC DRIF Research Initiative fund.

[12] Su, H.-J., and McCarthy, J. M., 2006, "A Polynomial Homotopy Formulation of the Inverse Static Analysis of Planar Compliant Mechanisms," *ASME Journal of Mechanical Design*, 128(4):776-786.

## References

- [1] Howell, L. L., 2001, *Compliant Mechanisms*, Wiley-Interscience.
- [2] Howell, L. L., and Midha A., 1995 "Parametric Deflection Approximations for End-Loaded, Large-Deflection Beams in Compliant Mechanisms," *ASME Journal of Mechanical Design*, 117(1):156-165.
- [3] Howell, L.L., 1991, "The Design and Analysis of Large-Deflection Members in Compliant Mechanisms," M.S. Thesis, Purdue University, West Lafayette, Indiana.
- [4] Saxena, A., and Kramer, S. N., 1998 "A Simple and Accurate Method for Determining Large Deflections in Compliant Mechanisms Subjected to End Forces and Moments," *ASME Journal of Mechanical Design*, 120(3):392-400.
- [5] Lyon, S. M., Howell, L. L., Roach, G. M., 2000, "Modeling Fixed-Fixed Flexible Segments via the Pseudo-Rigid-Body Model," *Proceedings of the ASME Dynamics and Control Division*, at the 2000 ASME International Mechanical Engineering Congress and Exposition, Orlando, FL, Nov. 5-10, DSC-Vol. 69-2, pp. 883-990.
- [6] Saggere, L. and Kota, S., 2001, "Synthesis of Planar, Compliant Four-Bar Mechanisms for Compliant-Segment Motion Generation," *ASME Journal of Mechanical Design*, 123(4):535-541.
- [7] Saxena, A., 1997, "A New Pseudo-Rigid-Body Model for Flexible Members in Compliant Mechanisms," *Masters Thesis*, University of Toledo, Toledo, OH, USA.
- [8] Roark, R.J. and Young, W.C., 1982, *Formulas for Stress and Strain*, McGraw-Hill, New York.
- [9] Howell, L. L., Midha A., and Norton, T. W., 1996, "Evaluation of Equivalent Spring Stiffness for Use in a Pseudo-Rigid-Body Model of Large-Deflection Compliant Mechanisms," *ASME Journal of Mechanical Design*, 118(1):126-131.
- [10] Su, H. J., and McCarthy, J. M., 2007, "Synthesis of Bistable Compliant Four-Bar Mechanisms Using Polynomial Homotopy," *ASME Journal of Mechanical Design*, 129(10):1094-1098.
- [11] Tsai, L. W., 1999, *Robot Analysis, The Mechanics of Serial and Parallel Manipulators*, Wiley-Interscience.